Photoelectron imaging of PtI_2^- and its PtI^- photodissociation product.

Jemma A. Gibbard and Jan. R. R. Verlet*

Department of Chemistry, Durham University, Durham DH1 3LE, United Kingdom

Abstract

The photoelectron imaging of PtI_2^- is presented over photon energies ranging from $h\nu$ = 3.2 to 4.5 eV. The electron affinity of PtI_2 is found to be 3.4±0.1 eV and the photoelectron spectrum contains three distinct peaks corresponding to three low-lying neutral states. Using a simple d-block model, and the measured photoelectron angular distributions, the three states are tentatively assigned. Photodissociation of PtI_2^- is also observed, leading to the formation of I^- and of PtI^-. The latter allows us to determine the electron affinity of PtI to be 2.35±0.10 eV. The spectrum of PtI^- is similarly structured with three peaks which, again, can be tentatively assigned using a similar model that agrees with the photoelectron angular distributions.

*jemma.gibbard@durham.ac.uk

Introduction

Platinum halides have complex electronic structures and exhibit unusual bonding, resulting in very high electron affinities (EA) and high formal oxidation states on the platinum core. These properties have led platinum halides to be investigated as superhalogens and small multiply charged anions. For example, $[PtCl_4]^{2-}$ is the smallest experimentally reported dianion[1] and PtF_6 has an EA of ~7 eV and oxidises both O_2 and Xe.[2-4] To date, the focus has been on platinum fluorides, chlorides and – to a lesser extent – bromides, with no gas-phase studies investigating the electronic structure of the platinum iodides.[5-7] Hence, there are unanswered questions about how the interesting properties that characterise the smaller platinum halides, evolve for larger halogens, especially as changes are observed for more elaborate platinum complexes, such as $[PtX_3(C_2H_4)]^-$ where X is Cl, Br or I, with larger halide ligands.[8, 9] In addition to the increased size of iodine, which may induce steric strain into the molecular framework, iodine has a larger spin-orbit splitting and a higher polarizability, which may change the bonding and electronic structure of the platinum iodides compared to other platinum halides. Whilst building an understanding of the evolution of the electronic structure of the platinum halides is of fundamental interest; platinum halides have also found applications in catalytic processes. For example, perovskites with $Pt\text{-}I_3$ active sites are highly efficient photocatalysts for H_2 production.[10] Here, we study the electronic structure and photochemistry of the simplest platinum iodides, PtI^- and PtI_2^-. We employ photoelectron imaging, which probes the electronic structure directly and, through its photoelectron angular distributions, also offers insight into the molecular orbitals involved. Performing photoelectron imaging over a range of photon energies can often provide more insight into the electron loss dynamics, as we and others have shown in several cases, and we use a similar approach here.[11-17]

The photoelectron angular distributions (PADs) are particularly interesting in the context of metal complexes, where, in principle, the sensitivity to the electronic structure can provide insight into the chemical bonding involved.[18-20] Jarrold and coworkers have recorded photoelectron spectra for some transition metal and lanthanide clusters, including NiO^- and Gd_2O^-, at different laser polarisations relative to the detector, in order to gain some information about the PADs and characterise the spectroscopic transitions.[21, 22] Here, we record the full PADs, using photoelectron imaging, in order to investigate the symmetry of the molecular orbitals of transition metal complexes. Moreover, for the case of platinum iodides, spin-orbit coupling and relativistic effects are likely to be large and these can have striking influences on the molecular orbitals of such complexes, which again the PADs may be sensitive to.[23, 24]

Previous studies have considered the electronic structure of platinum fluorides and chlorides, PtF_n^- and $PtCl_n^-$ (n = 1 – 8), using theoretical methods and photoelectron spectroscopy.[5, 6] Strong similarities were noted between the platinum fluorides and chlorides. Both platinum dihalides exhibited linear anion and neutral ground states. The EA for PtF_2 was calculated to be between 2.72 – 3.13 eV,[6] which is slightly lower than the experimentally measured EA ~ 3.5 eV for $PtCl_2$.[5] The previous photoelectron spectroscopic study of $PtCl_n^-$ (n = 2, 4 and 5) used a single photon energy $h\nu$ = 4.66 eV; the $PtCl_2^-$ spectrum comprised of three distinct bands.[5] Note that the n = 1 diatomic molecule was not observed in this previous work and, to the best of our knowledge, there have been no photoelectron spectra of any platinum halide reported. In general, stable MX molecules are rare, and typically require a d^{10} electron configuration and bulky ligands in order to stabilise the cluster.[25] Here, photodissociation of PtI_2^- results in PtI^- and has allowed us to measure the photoelectron spectrum of a diatomic platinum halide for the first time.

Experimental methods

Our work utilises 2D photoelectron imaging and the experimental apparatus has been described in detail elsewhere.[26, 27] Briefly the anions were produced via electrospray ionisation of a solution of 2 mMol K_2PtI_6 in methanol. Anions were desolvated in a capillary, transferred through a series of differentially pumped regions by means of ring-electrode guides, and stored in a ring electrode trap, before being accelerated and mass-selected in a Wiley-Mclaren time-of-flight spectrometer. The ring-electrode guides also serve to perform collision-induced dissociation.[26, 27] In the present experiments, PtI_6^{2-} serves as a precursor to form other platinum iodide species, with PtI_2^- being one of the most abundant in the mass-spectrum. As described below, PtI^- was formed via the photodissociation of PtI_2^-. Surprisingly, we did not observe PtI_6^{2-}, suggesting that it may be quite unstable as an isolated dianion.

Photoelectrons were generated through the intersection of the mass-selected anion packet and a nanosecond laser pulse. Pulses of variable photon energies in the visible and UV were produced via a Nd:YAG pumped optical parametric oscillator (OPO). The photoelectrons were imaged on a dual microchannel plate detector in a velocity map imaging configuration,[28] and photoelectron spectra were subsequently obtained from these raw images. Photoelectron imaging also yields the PADs of the emitted electron relative to the polarisation axis, which was parallel to the detector face. Previous studies of platinum halides used a magnetic bottle electron detector, which does not record the PAD and has a very low detection efficiency for photoelectrons with low electron kinetic energy (eKE).[5, 21, 29] The energy resolution of our photoelectron spectrometer is 5% of the eKE, based on calibration with the photodetachment of iodide.

Analysis

The raw photoelectron images were deconvoluted with a polar onion-peeling algorithm,[30] which reconstructs the 3D Newton sphere of electrons from the 2D image obtained and consequently recovers both the photoelectron spectra and PADs. The PADs are dictated by the molecular orbital from which the electron is removed in the photodetachment process. The emission yield, I, as a function of angle, θ, between the outgoing electron vector and the polarisation vector of the light field, $\boldsymbol{\varepsilon}$, can be expressed as $I(\theta) \propto [1 + \beta_2 P_2(\cos\theta)]$, where $P_2(\cos\theta)$ is the second order Legendre polynomial and β_2 is a so-called anisotropy parameter.[18, 19] This latter parameter defines the PAD and is restricted between the values $-1 \leq \beta_2 \leq 2$. When $\beta_2 = -1$, the emission is predominantly perpendicular to $\boldsymbol{\varepsilon}$ ($I(\theta) \propto \sin^2\theta$) and when $\beta_2 = 2$, it is predominantly parallel to $\boldsymbol{\varepsilon}$ ($I(\theta) \propto \cos^2\theta$). When $\beta_2 = 0$, the emission is isotropic.

Results

Photoelectron spectra of PtI_2^- were recorded with nanosecond (ns) laser pulses at photon energies between $h\nu$ = 3.2 – 4.5 eV. Figure 1 shows two representative photoelectron images of PtI_2^- recorded at $h\nu$ = 3.6 and 4.2 eV, from which subsequent photoelectron spectra have been extracted. All the photoelectron spectra are shown in Figure 2 and reported as a function of electron binding energy (eBE), where eBE = $h\nu$ – eKE. The spectra are normalised to the most intense feature in each spectrum, averaged using a five-point moving mean and are offset to allow comparison. There are several spectral features that are clearly visible over different ranges of photon energies. These can be broadly classed into three distinct groups: we have colour-coded these in Figure 2 and labelled as A, B, and C, in order of decreasing eBE. We now consider these in turn.

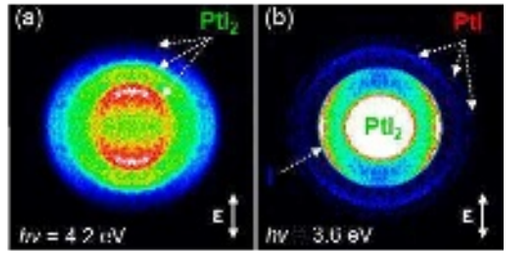

Figure 1: Photoelectron images for PtI_2^- recorded with ns laser pulses at a) $h\nu$ = 4.2 eV and b) $h\nu$ = 3.6 eV. Individual rings are assigned to photodetachment from the anion of the indicated species. In b), the photoelectron signal is saturated near the centre of the image to allow the outer rings, that are attributable to the photodetachment of PtI^-, to be visible. The polarisation axis of the light is indicated by the vertical double arrow.

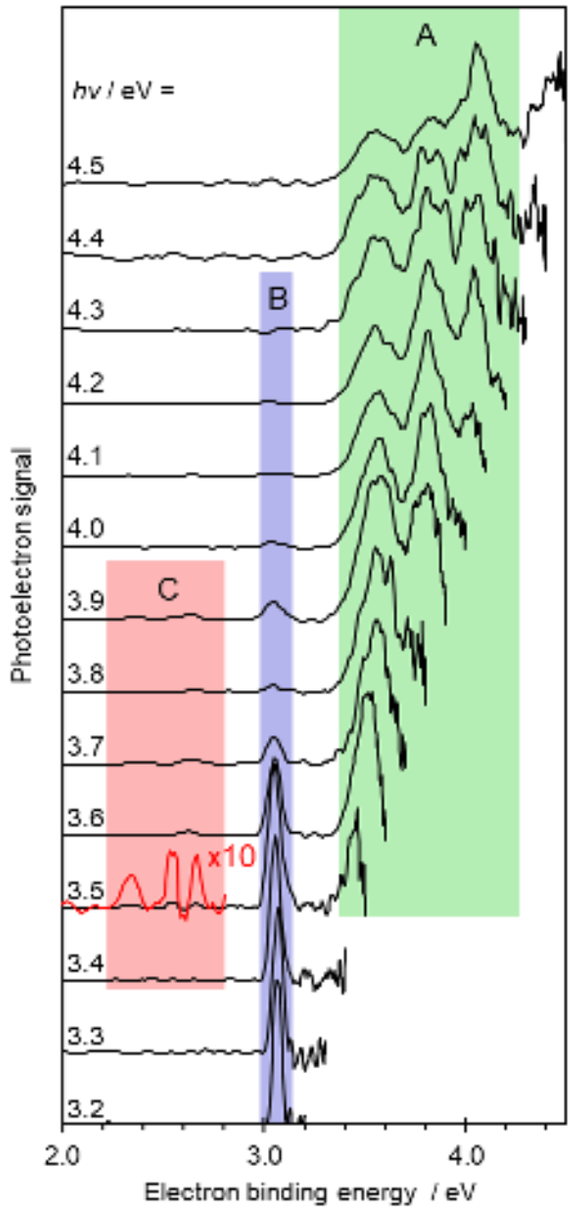

Figure 2: Photoelectron spectra of PtI_2^- recorded with $h\nu$ = 3.2 eV – 4.5 eV and presented as a function of electron binding energy (eBE). All spectra are normalised to the largest peak and offset for clarity. Direct detachment channels of PtI_2^- are labelled as A and highlighted in green. Photodissociation and subsequent photodetachment of I^- is labelled as B and highlighted in blue. Photodissociation and subsequent photodetachment of PtI^- is labelled as C and highlighted in red. The photoelectron spectrum of PtI^- recorded at $h\nu$ = 3.5 eV is multiplied by a factor of 10 to accentuate its photoelectron signal and is shown in red.

A, *Direct detachment*: For $h\nu$ > 4.1 eV, a cluster of three distinct peaks can be seen with maxima at eBE ~ 3.5, 3.8 and 4.0 eV. The three peaks can be assigned to direct detachment: $PtI_2^- + h\nu \rightarrow PtI_2(E_{int}) + e^-$, where E_{int} accounts for the fact that the PtI_2 can be produced with varying degrees of internal energy. Within our spectral resolution, this internal energy can take the form of vibrational or electronic energy. The distribution of the peaks does not follow a clear Franck-Condon progression and the peak spacing is much larger than may be expected for the low frequency vibrations typical of heavy triatomic molecules (c.f. 14 meV for the symmetric stretch of I_3).[31] Moreover, the three direct detachment bands have different measured β_2 values. From the $h\nu$ = 4.4 eV photoelectron image, we determine β_2 to be −0.9, +0.3 and +0.4. Such dramatic changes are inconsistent with a vibrational progression. Hence, we conclude that the distinct peaks correspond to the formation of the neutral PtI_2 in different electronic states, where the differing β_2 values indicate detachment involving different molecular orbitals. As the photon energy decreases below 4.1 eV, the higher eBE features are no longer accessible. The $h\nu$ = 4.1 eV spectrum, in particular, clearly shows the effect of the reduced detachment cross section at low eKE. Additionally, as threshold is approached the features have β_2 ~ 0. Both these observations are expected from the Wigner law.[32] The maximum of the peak with the lowest binding energy of the three peaks offers the vertical detachment energy, VDE = 3.5±0.1 eV, and its onset offers the adiabatic detachment energy (electron affinity), ADE = 3.4±0.1 eV.

B, *Iodide detachment*: For photon energies less than approximately 4.0 eV, a new feature emerges peaking at eBE = 3.06 eV. This feature grows in relative intensity as the photon energy decreases, but this is likely just a reflection of the decreasing cross section of the direct features (A) discussed above. The feature becomes much less prominent for $h\nu$ > 3.9 eV and remains visible down to 3.2 eV. The spectral shape, binding energy and β_2 parameters of peak B are consistent with the well-known photoelectron spectrum of I^-.[33] This detachment peak is presumably formed via a multiple-photon process involving the two steps of photodissociation and subsequent photodetachment (here, we will use the term two-photon to describe such a process),

$$PtI_2^- + h\nu \rightarrow PtI + I^- ,$$

$$I^- + h\nu \rightarrow I + e^- .$$

The presence of two-photon photodissociation and photodetachment of the resulting I^-, below the ADE of PtI_2^-, requires the presence of at least one *bound* electronic state of the anion, which is excited by the first photon. Dissociation may occur on the excited state potential energy surface or on the ground state surface following internal conversion; we cannot obtain information about the mechanism from our current experiments. As $h\nu$ increases, direct detachment also becomes possible so that the anion excited states are now in the detachment continuum (*i.e.* resonances) and dissociation will compete with autodetachment.[17, 34-37] The relative decrease of the intensity of the I^- feature compared to the direct detachment channels of PtI_2^- can arise from a number of reasons in addition to the one noted above: the favourability of a one-photon process over two-photon process, the large apparent photodetachment cross-section of PtI_2^-, and the absorption profile to the excited states of PtI_2^-. At the low-energy spectral end, we did not succeed in acquiring a spectrum at $h\nu$ = 3.1 eV, in part because our OPO has very weak output here and the cross section for detachment from iodide is low (near-

threshold). Below $h\nu$ = 3.06 eV, iodide would no longer be visible in our experiment. Hence, we cannot comment on the spectral range of the excited state absorption of PtI_2^-, except to say that it spans at least $3.2 \leq h\nu \leq 4.0$ eV.

C, *Platinum Iodide detachment*: Finally, we also noted the presence of a very weak signal in several of the photoelectron images. Figure 1 highlights this at $h\nu$ = 3.6 eV, where a series of sharp rings are seen at large radii. In Figure 2, these features are not immediately obvious because of their low intensity, but we highlight it in the $h\nu$ = 3.5 eV photoelectron spectrum by scaling the signal in the relevant range by an order of magnitude. The low intensity of this feature suggests that it arises from another two-photon photodissociation and subsequent photodetachment process (similar to feature B). These peaks are present over the spectral range $3.4 \leq h\nu \leq 3.9$ eV, but with the largest intensity at $h\nu$ = 3.5 eV and 3.6 eV. The overall structure, at $h\nu$ = 3.5 eV and 3.6 eV, consists of three distinct peaks with eBE = 2.35 – 2.80 eV. Each peak has a different anisotropy i.e. $\beta_2 = -0.8$, +2.0 and +1.5 in order of increasing eBE and extracted from the $h\nu$ = 3.5 eV spectrum. However, we do note that the signal level for these features is very low, such that the spectral structure and the PADs, should be taken as qualitative rather than quantitative measurements.

As only Pt and I is present in PtI_2^-, we first considered the possibility that the photodissociation product corresponds to Pt^-, which is subsequently detached. However, the electron affinity of Pt has been measured as 2.12 eV, and the previously reported photoelectron spectrum shows different structure and relative intensity,[38, 39] so the spectrum is not consistent with this explanation. The photoelectron spectrum measured is also not consistent with that of I_2^-, which has been extensively studied.[40] This leaves us with the only other alternative, PtI^-. To the best of our knowledge, this diatomic has not been characterised, either as an anion or

neutral molecule. From our spectra, we determine that the ADE = 2.35±0.10 and the VDE = 2.45±0.1 eV.

Analogous to feature B, the most likely explanation for this feature is the two-photon process:

$$PtI_2^- + h\nu \rightarrow PtI^- + I\,,$$

$$PtI^- + h\nu \rightarrow PtI + e^-.$$

Hence, the excited anionic states accessed in PtI_2^- appear to lead to a competition between dissociation leaving the negative charge on the PtI or I, with the latter apparently dominating (although this is difficult to verify without knowledge of relative photodetachment cross sections of the anions). It may also be possible that PtI^- undergoes dissociation (either spontaneous or by absorption of a further photon) to form I^-, and this would be indistinguishable spectroscopically from the two-photon process of photodissociation of PtI_2^- to form I^-, although a photodissociation would be unlikely by the small probability of a three-photon process required.

The three peaks associated with the photodetachment from PtI^- with differing β_2 values are similar to the photodetachment from PtI_2^- (feature A). The spectral structure of the direct detachment channels for PtI^- and PtI_2^- both exhibit three peaks, with a $\beta_2 < 0$, > 0 and > 0, and a total width of ~1 eV. This is perhaps unexpected as the electron configurations of the two molecules are different: PtI^- is an even-electron species whereas PtI_2^- is an odd-electron species.

Discussion

The direct photoelectron spectrum of PtI^- shares many characteristics of that seen for PtI_2^-. Our measured ADE (and VDE) are also similar to those calculated values for $PtCl^-$ (VDE = 2.21 to 2.70 eV, depending on level of theory),[5] the only other diatomic platinum halide studied to date. As we were not able to form an ion beam of PtI^- directly via electrospray ionization, it is difficult to determine whether it undergoes photodissociation. However, this may be unlikely as ionic photodissociation could result in a neutral Pt atom, which is not a favoured oxidation state of platinum.

Previous photoelectron spectroscopy of $PtCl_2^-$ determined its ADE = 3.5 eV and its VDE = 3.83 eV,[5] while computational work predicted the electron affinity of PtF_2 to be between 2.72 – 3.13 eV depending on the level of theory used.[6] Our measured VDE = 3.5 eV for PtI_2^-, is therefore of similar magnitude to these lighter halides. Clear similarities are also observed between the photoelectron spectra of PtI_2^- and $PtCl_2^-$.[5] The $h\nu$ = 4.66 eV photoelectron spectrum of $PtCl_2^-$ exhibits three distinct peaks due to direct detachment. The highest eBE peak was near threshold and its low relative intensity may be skewed by threshold effects, as we noted in the $h\nu$ = 4.1 eV spectrum in Figure 2 for example. The two other peaks at lower eBE are well-resolved and the overall width of the observed photoelectron signal spanning the three peaks is approximately 1 eV. This overall appearance is similar to the photoelectron spectra observed for PtI_2^- (e.g. see Figure 2 spectrum at $h\nu$ > 4.1 eV, which has three sharp features with a total spectral width of ~1 eV). The ~1 eV total spectral width of the direct detachment bands for the dichloride and diiodide platinum complexes indicates that the electronic states in the neutral are not just spin-orbit split states arising from the spin-orbit coupling involving the halide.

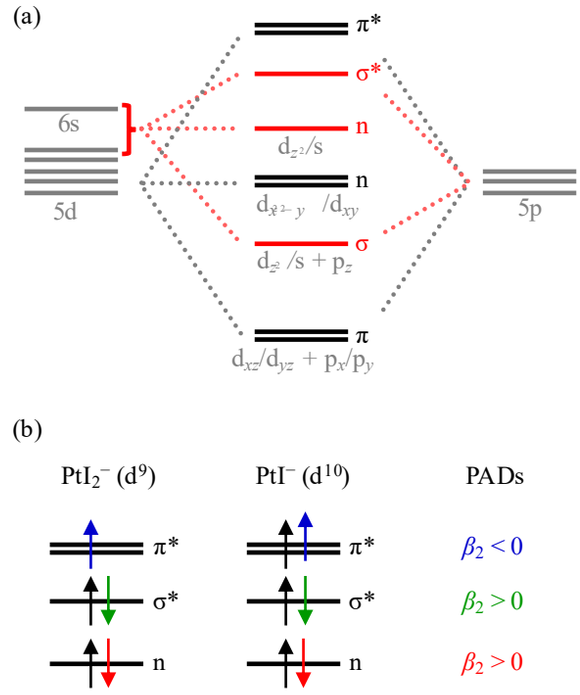

Figure 3: (a) Molecular orbital (MO) picture of PtI_2^-, involving the d-block model orbitals, in which the platinum 5d and 6s orbitals mix with the 5p orbitals on iodide. The red states indicate the MOs arising from the hybridisation of the 6s with the $5d_{z2}$ orbital on platinum that mixes with the $5p_z$ on iodine. (b) d-block diagram showing the 3 highest lying occupied MOs together with their occupancy for PtI_2^- and PtI^-. Removal of the blue, green, or red electrons in a photodetachment process produces the corresponding neutral excited states and leads to a PAD that can be described by the β_2 parameters indicated on the right.

To assign the three lowest lying electronic states of the neutral, we will focus on a simple molecular orbital (MO) picture for typical d-block compounds and refrain from performing ab initio calculations because of the large spin-orbit coupling and relativistic effects that are poorly accounted for in standard electronic structure calculations. In the d-block model, the *n*d valence orbitals of a transition metal, as well as any (*n* + 1)p and (*n* + 1)s orbitals with the correct symmetry to mix, are considered along with a symmetric ligand field based on an undercoordinated octahedral geometry.[25] From this model, a picture of the non-bonding and anti-bonding orbitals, which are typically the highest energy occupied orbitals and strongly localised on the metals can be developed, where the energies of the d-orbitals are determined

by overlap with the ligand field. With reference to Figure 3(a), the d_{x2-y2} and d_{xy} on Pt cannot interact with the atomic orbitals on I and forms a pair of degenerate non-bonding (n) MOs. The overlap between the d_{xz} and p_x as well as the d_{yz} and p_y orbitals will form doubly degenerate π and π* MOs. In the absence of orbital mixing, the overlap of the d_{z2} and ligand localised p_z orbitals may be expected to lead to σ and σ* MOs. However, the 6s orbital of Pt is close in energy to the 5d orbitals, as evidenced by the $5d^9\ 6s^1$ ground state electron configuration of Pt, and of the correct symmetry to mix with the $5d_{z2}$ orbital, leading to a hybrid s/d orbital. This hybrid orbital in turn interacts with the p_z orbital on I to lead to three MOs: one bonding, one antibonding and one non-bonding, as shown in Figure 3(a) in red. These MOs, while being hybrid, effectively appear as σ-type MOs.

Taking the above arguments and applying it to the case of a linear ML_2 molecule with a σ bond and the potential for π interactions, as is the case for the d^9 PtI_2^- complex, the d-block is split into four (n, n, σ* and π*). From a simple Koopmans' theory picture, electron loss from any of these orbitals in PtI_2^- could result in the formation of distinct neutral states, and therefore a band in the photoelectron spectra. As three bands are observed in the photoelectron spectra (Figure 2), the three highest energy MOs of the d-block of PtI_2^- which are likely to contribute to the photodetachment dynamics, are shown in Figure 3(b). Both the antibonding and non-bonding s/d hybrid orbitals are filled and one additional electron resides in the π* orbital (i.e. PtI_2^- is an open-shell radical). However, photodetachment from the lowest energy n MOs in the d-block (based on the d_{x2-y2} and d_{xy} platinum orbitals) are not observed in the photoelectron spectra, suggesting that there is insufficient energy to remove an electron from this MO. This may be surprising given the similar energy of the Pt 6s and 5d but the d-block model is likely to be an oversimplified picture of the MOs, meaning the energy difference between the n orbitals, one of which is a hybridised MO, is likely to be larger than implied in the simple

model. Alternatively, the n orbitals are near-degenerate and both contribute to the highest eBE peak.

We additionally have measured the PADs for the three individual direct detachment peaks. Detailed qualitative and semi-quantitative models have been developed for the prediction of the β_2 parameter.[41-43] Given the qualitative picture presented above, we continue along such lines and consider the qualitative PADs that might be expected for the three different detachment channels. Qualitatively, β_2 parameters are expected to be positive or negative depending on the nature of the orbital from which the electron is detached. Generally, for a σ orbital, the outgoing wave can be approximated as a p-wave resulting in $\beta_2 > 0$; in contrast, for a π orbital, the outgoing wave will have a mixture of s- and d-waves which results in $\beta_2 < 0$. For the three channels observed in the experiment, we observe $\beta_2 = -0.9$ for removal from the π* MO; $\beta_2 = +0.3$ eV for the removal from the σ* hybrid MO; and $\beta_2 = +0.4$ eV for the removal from the n MO. These observations are in qualitative agreement with the expectation assuming that the highest eBE peak arises from the n-hybrid MO. The PADs therefore offer additional support that the proposed assignment and simple d-block picture is representative of the electronic structure of PtI_2^-. It should be noted that the origin of the structure of the $PtCl_2^-$ photoelectron spectrum was not discussed by Joseph *et al*..[5]

In this simple d-block model we have not accounted for the role of spin multiplicities, which would allow the observed spectral structure and PADs for PtI_2^- to be explained via photodetachment from just two MOs, instead of the three suggested by the above model. Specifically, the three bands could arise due to removal of an electron from the π*, which would produce a $^1\Sigma$ neutral state, or from the σ*, which would produce $^1\Pi$ and $^3\Pi$ neutral states. The observed PADs would also be consistent with this model, as the two bands originating from electron removal from the same σ* would both have $\beta_2 > 0$.

However, the d-block model shown in figure 3(b), with or without the inclusion of spin multiplicities, does not consider the role of spin-orbit coupling, which may have a large effect on the nature and energies of the valence MOs of PtI_2^-. For example, consider the addition of Russell-Saunders (LS) spin-orbit coupling to the HOMO and HOMO–1 of the simple d-block and spin multiplicities model. In this picture the removal of an electron from the π* or σ* d-block orbitals, could result in $^1\Sigma_0$, $^1\Pi_1$, $^3\Pi_0$, $^3\Pi_1$ or $^3\Pi_2$ neutral states. In light of the large spin-orbit coupling observed in atomic iodine ($E(^2P_{3/2}) - E(^2P_{1/2}) = 0.94$ eV)[44] and platinum ($E(^3D_1) - E(^3D_3) = 1.25$ eV)[45], it may be expected that the different spin-orbit states of Π symmetry will have significantly different energies but, as the Π states originate from electron ejection from the same σ* orbital, the PADs may be expected to be similar (as in the spin multiplicities model described above). Therefore, this combined d-block model with spin-orbit coupling could also explain the origin of the three observed bands and the measured PADs for PtI_2^-. However, from this picture we may expect more bands in the photoelectron spectra of PtI_2^- than are observed (overlapping bands may not have been resolved). In addition, it is more difficult to explain the strong similarities between the photoelectron spectra of $PtCl_2^-$ and PtI_2^-, using this picture, as the Cl and I have significantly different spin-orbit splittings.

On a more fundamental note, it is questionable how valid the use of LS coupling is for PtI_2^-, when heavy atoms such as Pt are best described by J-J coupling and the d-block is localised on the metal core. It should be noted that J-J coupling would also result in four spin-orbit split neutral states following electron removal from the σ*. One further consideration is the effect of spin-orbit coupling on the PAD, particularly in the limit of J-J coupling, where the orbital angular momentum quantum number (L) is no longer a good quantum number. PADs are often qualitatively interpreted in terms of the L of the orbital from which the electron is lost, and therefore if J rather than L is well defined, it may be challenging to predict the PADs associated with specific photodetachment channels.

A very similar three-state d-block picture can be constructed for PtI^- (Figure 3(b)). The highest MOs being π*, followed by a σ* hybrid MO and the n hybrid MO. Formally, the d-block would also contain a lower energy n MO, but this is not observed here, either because it is too low in energy or because the peak in the photoelectron spectra is obscured by the much higher intensity I^- feature (B in figure 2). The hybridisation in PtI^- is slightly more complicated because there is likely to also be mixing with the 6p orbitals of the Pt atom. But overall, given the similarity between the photoelectron spectroscopy of PtI_2^- and PtI^-, our proposed picture appears appropriate. In Figure 3(b), the MO occupancy is also shown, along with the likely photodetachment channels that contribute to the photoelectron spectrum. Analogous to the PtI_2^- detachment, the three peaks come about from the detachment of the π *, σ* hybrid, and n hybrid MOs. The PADs are expected to be similar again: $\beta_2 < 0$, $\beta_2 > 0$ and $\beta_2 > 0$, respectively. This is again in excellent qualitative agreement with experiment. It should be noted that addition of spin multiplicities and spin-orbit coupling to this three-state d-block model does not readily describe the observed spectral structure of PtI^-, as LS coupling would predict two bands at the highest eBE with $\beta_2 < 0$.

Note that we specifically refrained from performing electronic structure calculations. This was done because of the lack of confidence we have in these, particularly for predicting the MOs that may be contributing to the detachment. Specifically, spin-orbit coupling, which in reality is likely to be intermediate in character between the limits of LS and J-J coupling, can lead to strong mixing of angular momenta. However, despite the likely large role spin-orbit effects have on the electronic structure of PtI_2^- and PtI^-, it is very challenging to accurately account for these effects in electronic structure calculations. Therefore, instead of attempting to provide interpretations based on electronic structure calculations in which we have little confidence, we prefer the simple d-block picture which we feel offers much more chemical insight too.

In addition to the direct photoelectron spectra of PtI_2^-, we also observe secondary (two-photon) detachment from I^- or PtI^-, indicating that bound (with respect to electron loss) electronically excited states for PtI_2^- exist (see Figure 2, feature B and C) and lead to two possible dissociation channels: I + PtI^- or I^- + PtI. From our experiments, we cannot gain any insight into the dynamics that leads to dissociation, and we cannot determine whether the dissociation occurs on the ground or the excited state. However, assuming that photodetachment from I^- and PtI^- have similar overall cross-sections, the photoelectron spectra in Figure 2 suggest that the I^- + PtI channel dominates. This observation is consistent with the fact that the electron affinity of iodine (3.059 eV) is larger than that of platinum iodide (2.35 eV).

Conclusion

A photoelectron imaging study of PtI_2^- is presented in the photon energy range $3.2 \leq h\nu \leq 4.5$ eV. The VDE of PtI_2^- is measured to be 3.5±0.1 eV and the electron affinity of PtI_2 is 3.4±0.1 eV. Three peaks contribute to the direct photoelectron spectrum, each with a distinct photoelectron angular distribution (PAD), which we can assign to the direct detachment from the anion to the three lowest lying electronic states of the neutral. Using a d-block molecular orbital model in which the 5d and the 6s orbitals on Pt interact with the 6p orbitals on I, a molecular orbital picture is constructed that is consistent with the observed spectrum including the PADs. The use of PADs to assign and understand the electronic structure of transition metal complexes holds significant potential in building up comprehensive pictures of such complexes.

PtI_2^- is also observed to undergo photodissociation to produce I^- predominantly, as evidenced by the photodetachment from iodide. This feature is visible over a large range of photon energies, including below the detachment threshold, indicating that PtI_2^- has at least

one bound excited state with respect to electron loss. In addition to the loss of I^-, additional features are seen over a spectral range near $h\nu$ ~ 3.5 eV. These have been assigned to PtI^- and a d-block model analogous to that for PtI_2^- allows us to assign the features and their PADs. The electron affinity of PtI is found to be 2.35±0.10 eV.

Acknowledgments

The authors would like to thank Dr. Basile Curchod for valuable discussions about the electronic structure of PtI_2^- and PtI^-. Jemma A. Gibbard is grateful for support from a Ramsay Memorial Fellowship.

Author Declarations

The authors have no conflicts to disclose.

Data availability statement

The data that support the findings of this study are available from the corresponding author upon reasonable request.

References

1. Wang, X.-B.; Wang, L.-S., Experimental Search for the Smallest Stable Multiply Charged Anions in the Gas Phase. *Phys. Rev. Lett.* **1999,** *83* (17), 3402-3405.
2. Bartlett, N.; Lohmann, D. H., Fluorides of the noble metals. Part II. Dioxygenyl hexafluoroplatinate(V), O_2 +[PtF_6]? *J. Chem. Soc. (Res.)* **1962**, 5253.
3. Bartlett, N., Xenon Hexafluoroplatinate(V) $Xe^+[PtF6]^-$. *Proc. Chem. Soc.* **1962,** (June), 218.
4. Christe, K. O., Bartlett's discovery of noble gas fluorides, a milestone in chemical history. *Chem. Comm.* **2013,** *49* (41), 4588.

5. Joseph, J.; Pradhan, K.; Jena, P.; Wang, H.; Zhang, X.; Jae Ko, Y.; Bowen Jr, K. H., Evolution of superhalogen properties in $PtCl_n$ clusters. *J. Chem. Phys.* **2012,** *136* (19), 194305.
6. Wesendrup, R.; Schwerdtfeger, P., Structure and Electron Affinity of Platinum Fluorides. *Inorg. Chem.* **2001,** *40* (14), 3351-3354.
7. Wang, X.-B.; Wang, L.-S., Photodetachment of free hexahalogenometallate doubly charged anions in the gas phase: $[ML_6]^{2-}$, (M=Re, Os, Ir, Pt; L=Cl and Br). *J. Chem. Phys.* **1999,** *111* (10), 4497-4509.
8. Hou, G.-L.; Wen, H.; Lopata, K.; Zheng, W.-J.; Kowalski, K.; Govind, N.; Wang, X.-B.; Xantheas, S. S., A Combined Gas-Phase Photoelectron Spectroscopic and Theoretical Study of Zeise's Anion and Its Bromine and Iodine Analogues. *Ange. Chem. Int. Ed.* **2012,** *51* (26), 6356-6360.
9. Hou, G.-L.; Govind, N.; Xantheas, S. S.; Wang, X.-B., Deviation from the trans-Effect in Ligand-Exchange Reactions of Zeise's Ions $PtCl_3(C_2H_4)^-$ with Heavier Halides (Br^-, I^-). *J. Phys. Chem. A* **2018,** *122* (5), 1209-1214.
10. Zhou, P.; Chen, H.; Chao, Y.; Zhang, Q.; Zhang, W.; Lv, F.; Gu, L.; Zhao, Q.; Wang, N.; Wang, J.; Guo, S., Single-atom Pt-I_3 sites on all-inorganic Cs_2SnI_6 perovskite for efficient photocatalytic hydrogen production. *Nat. Comm.* **2021,** *12* (1).
11. Mensa-Bonsu, G.; Lietard, A.; Tozer, D. J.; Verlet, J. R. R., Low energy electron impact resonances of anthracene probed by 2D photoelectron imaging of its radical anion. *J. Chem. Phys.* **2020,** *152* (17), 174303.
12. Lietard, A.; Mensa-Bonsu, G.; Verlet, J. R. R., The effect of solvation on electron capture revealed using anion two-dimensional photoelectron spectroscopy. *Nat. Chem.* **2021,** *13* (8), 737-742.
13. Lietard, A.; Verlet, J. R. R.; Slimak, S.; Jordan, K. D., Temporary Anion Resonances of Pyrene: A 2D Photoelectron Imaging and Computational Study. *J. Phys. Chem. A* **2021,** *125* (32), 7004-7013.
14. Mason, J. L.; Harb, H.; Taka, A. A.; Mcmahon, A. J.; Huizenga, C. D.; Corzo, H.; Hratchian, H. P.; Jarrold, C. C., Photoelectron Spectra of $Gd_2O_2^-$ and Nonmonotonic Photon-Energy-Dependent Variations in Populations of Close-Lying Neutral States. *J. Phys. Chem. A* **2021,** *125* (3), 857-866.
15. Jagau, T.-C.; Dao, D. B.; Holtgrewe, N. S.; Krylov, A. I.; Mabbs, R., Same but Different: Dipole-Stabilized Shape Resonances in CuF^- and AgF^-. *J. Phys. Chem. Lett.* **2015,** *6* (14), 2786-2793.
16. Laws, B. A.; Gibson, S. T.; Lewis, B. R.; Field, R. W., The dicarbon bonding puzzle viewed with photoelectron imaging. *Nat. Comm.* **2019,** *10* (1).
17. Anstöter, C. S.; Gartmann, T. E.; Stanley, L. H.; Bochenkova, A. V.; Verlet, J. R. R., Electronic structure of the para-dinitrobenzene radical anion: a combined 2D photoelectron imaging and computational study. *Phys. Chem. Chem. Phys.* **2018,** *20* (37), 24019-24026.
18. Cooper, J.; Zare, R. N., Angular Distribution of Photoelectrons. *J. Chem. Phys.* **1968,** *48* (2), 942-943.
19. Sanov, A., Laboratory-Frame Photoelectron Angular Distributions in Anion Photodetachment: Insight into Electronic Structure and Intermolecular Interactions. *Ann. Rev. Phys. Chem.* **2014,** *65* (1), 341-363.
20. Reid, K. L., Photoelectron Angular Distributions. *Ann. Rev. Phys. Chem.* **2003,** *54* (1), 397-424.
21. Moravec, V. D.; Jarrold, C. C., Study of the low-lying states of NiO^- and NIO using anion photoelectron spectroscopy. *J. Chem. Phys.* **1998,** *108* (5), 1804-1810.
22. Mason, J. L.; Harb, H.; Abou Taka, A.; Huizenga, C. D.; Corzo, H. H.; Hratchian, H. P.; Jarrold, C. C., New Photoelectron–Valence Electron Interactions Evident in the Photoelectron Spectrum of Gd_2O^-. *J. Phys. Chem. A* **2021,** *125* (45), 9892-9903.
23. Walker, T. E. H.; Waber, J. T., Spin-orbit coupling photoionization. *J. Phys. B: At. Mol. Phys.* **1974,** *7* (6), 674-692.
24. Pyykko, P., Relativistic effects in structural chemistry. *Chem. Rev.* **1988,** *88* (3), 563-594.
25. Jean, Y., *Molecular orbitals of transtion metal complexes*. OUP: 2005.

26. Lecointre, J.; Roberts, G. M.; Horke, D. A.; Verlet, J. R. R., Ultrafast Relaxation Dynamics Observed Through Time-Resolved Photoelectron Angular Distributions. *J. Phys. Chem. A* **2010,** *114* (42), 11216-11224.
27. Stanley, L. H.; Anstöter, C. S.; Verlet, J. R. R., Resonances of the anthracenyl anion probed by frequency-resolved photoelectron imaging of collision-induced dissociated anthracene carboxylic acid. *Chem. Sci.* **2017,** *8* (4), 3054-3061.
28. Horke, D. A.; Roberts, G. M.; Lecointre, J.; Verlet, J. R. R., Velocity-map imaging at low extraction fields. *Rev. Sci. Instrum.* **2012,** *83* (6), 063101.
29. Kruppa, S. V.; Nosenko, Y.; Winghart, M.-O.; Walg, S. P.; Kappes, M. M.; Riehn, C., Fragmentation pathways of dianionic $[Pt_2(\mu\text{-}P_2O_5H_2)_4+X,Y]^{2-}$ (X,Y=H, K, Ag) species in an ion trap induced by collisions and UV photoexcitation. *Int. J. Mass Spec.* **2016,** *395*, 7-19.
30. Roberts, G. M.; Nixon, J. L.; Lecointre, J.; Wrede, E.; Verlet, J. R. R., Toward real-time charged-particle image reconstruction using polar onion-peeling. *Rev. Sci. Instrum.* **2009,** *80* (5), 053104.
31. Taylor, T. R.; Asmis, K. R.; Zanni, M. T.; Neumark, D. M., Characterization of the I_3 radical by anion photoelectron spectroscopy. *J. Chem. Phys.* **1999,** *110* (16), 7607-7609.
32. Wigner, E. P., On the Behavior of Cross Sections Near Thresholds. *Phys. Rev.* **1948,** *73* (9), 1002-1009.
33. Davis, A. V.; Wester, R.; Bragg, A. E.; Neumark, D. M., Time-resolved photoelectron imaging of the photodissociation of I_2^-. *J. Chem. Phys.* **2003,** *118* (3), 999-1002.
34. West, C. W.; Bull, J. N.; Verlet, J. R. R., Charged Particle Imaging of the Deprotonated Octatrienoic Acid Anion: Evidence for a Photoinduced Cyclization Reaction. *J. Phys. Chem. Lett.* **2016,** *7* (22), 4635-4640.
35. Mensa-Bonsu, G.; Tozer, D. J.; Verlet, J. R. R., Photoelectron spectroscopic study of $I^-{\cdot}ICF_3$: a frontside attack S_N2 pre-reaction complex. *Phys. Chem. Chem. Phys.* **2019,** *21* (26), 13977-13985.
36. Gibbard, J. A.; Castracane, E.; Continetti, R. E., Photoelectron–photofragment coincidence spectroscopy of the mixed trihalides. *J. Chem. Phys.* **2020,** *153* (5), 054304.
37. Gibbard, J. A.; Castracane, E.; Krylov, A. I.; Continetti, R. E., Photoelectron photofragment coincidence spectroscopy of aromatic carboxylates: benzoate and *p*-coumarate. *Phys. Chem. Chem. Phys.* **2021,** *23* (34), 18414-18424.
38. Hotop, H.; Lineberger, W. C., Dye-laser photodetachment studies of Au^-, Pt^-, PtN^-, and Ag^-. *J. Chem. Phys.* **1973,** *58* (6), 2379-2387.
39. Zhang, X.; Liu, G.; Meiwes-Broer, K. H.; Ganteför, G.; Bowen, K., CO_2 Activation and Hydrogenation by PtH_n^- Cluster Anions. *Angew. Chem. Int. Ed.* **2016,** *55* (33), 9644-9647.
40. Zanni, M. T.; Taylor, T. R.; Greenblatt, B. J.; Soep, B.; Neumark, D. M., Characterization of the I_2^- anion ground state using conventional and femtosecond photoelectron spectroscopy. *J. Chem. Phys.* **1997,** *107* (19), 7613-7619.
41. Oana, C. M.; Krylov, A. I., Cross sections and photoelectron angular distributions in photodetachment from negative ions using equation-of-motion coupled-cluster Dyson orbitals. *J. Chem. Phys.* **2009,** *131* (12), 124114.
42. Simons, J., Ejecting Electrons from Molecular Anions via Shine, Shake/Rattle, and Roll. *J. Phys. Chem. A* **2020,** *124* (42), 8778-8797.
43. Anstöter, C. S.; Verlet, J. R. R., Modeling the Photoelectron Angular Distributions of Molecular Anions: Roles of the Basis Set, Orbital Choice, and Geometry. *J. Phys. Chem. A* **2021,** *125* (22), 4888-4895.
44. Luc-Koenig, E.; Morillon, C.; Vergès, J., Etude Expérimentale et Théorique de l'Iode Atomique.Observation du Spectre d'Arc Infrarouge, Classification et Structure Hyperfine. *Physica Scripta* **1975,** *12* (4), 199-219.
45. Blaise, J.; Vergès, J.; Wyart, J. F.; R. Engleman, J., Energy levels of neutral platinum (Pt I). *J. Phys. II France* **1992,** *2* (4), 947-957.

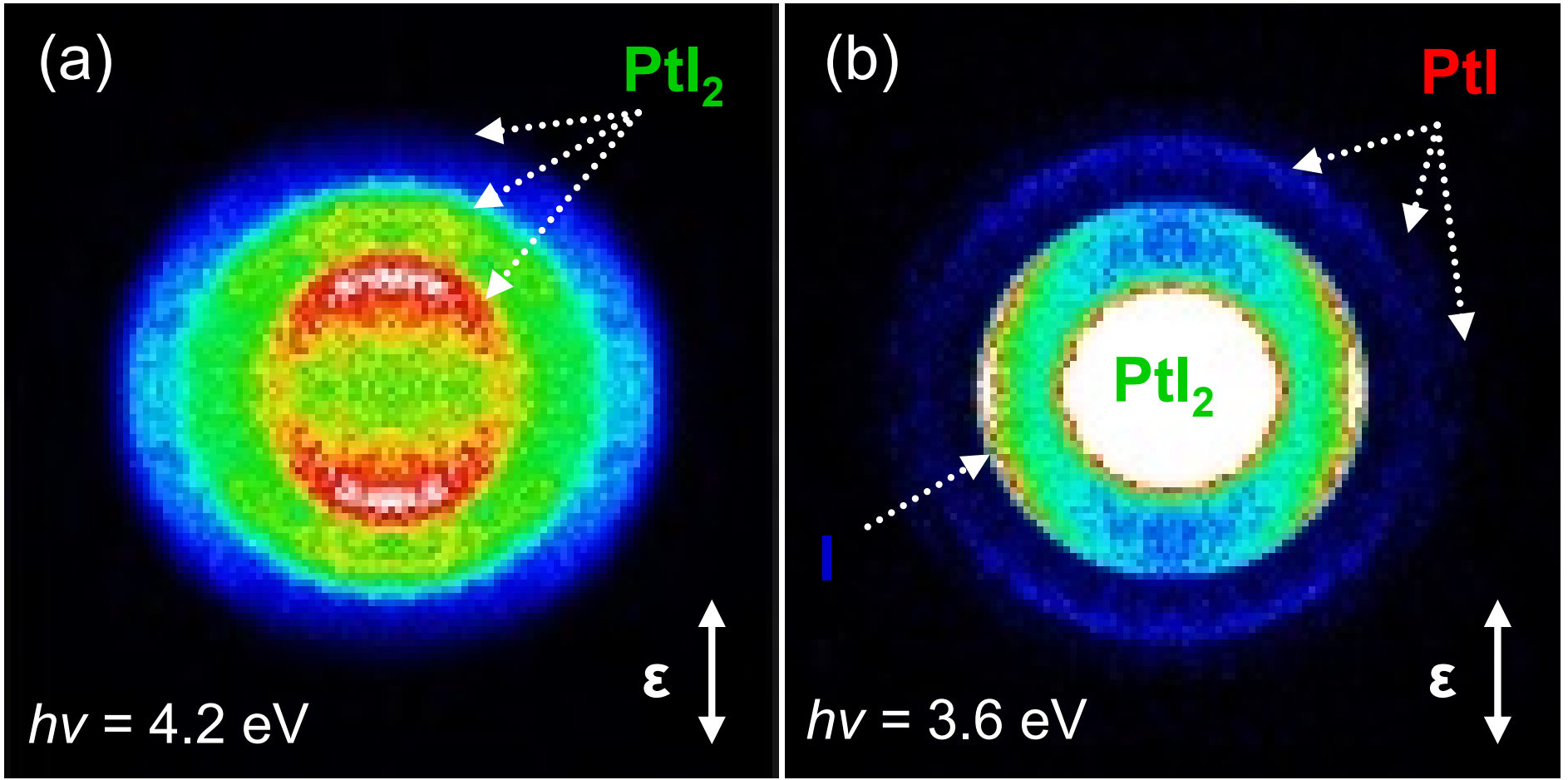
(a)
PtI2
hv = 4.2 eV
ε
(b)
PtI
PtI2
I
hv = 3.6 eV
ε

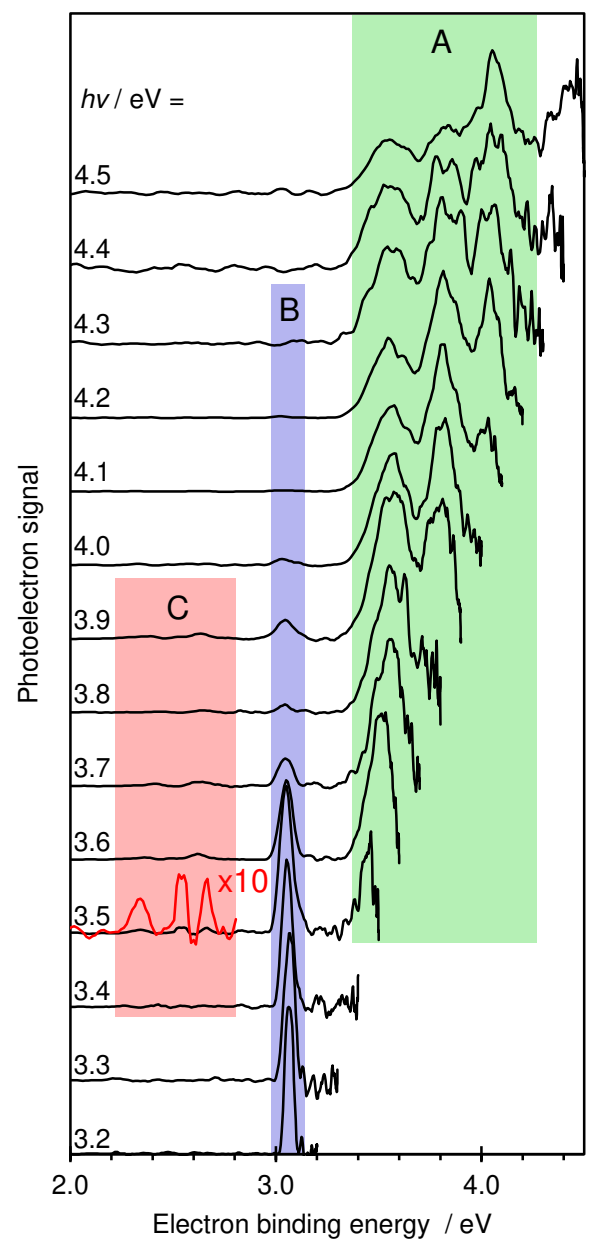
A
B
C
hv / eV =
4.5
4.4
4.3
4.2
4.1
4.0
3.9
3.8
3.7
3.6
3.5
3.4
3.3
3.2
x10
Photoelectron signal
2.0
3.0
4.0
Electron binding energy / eV

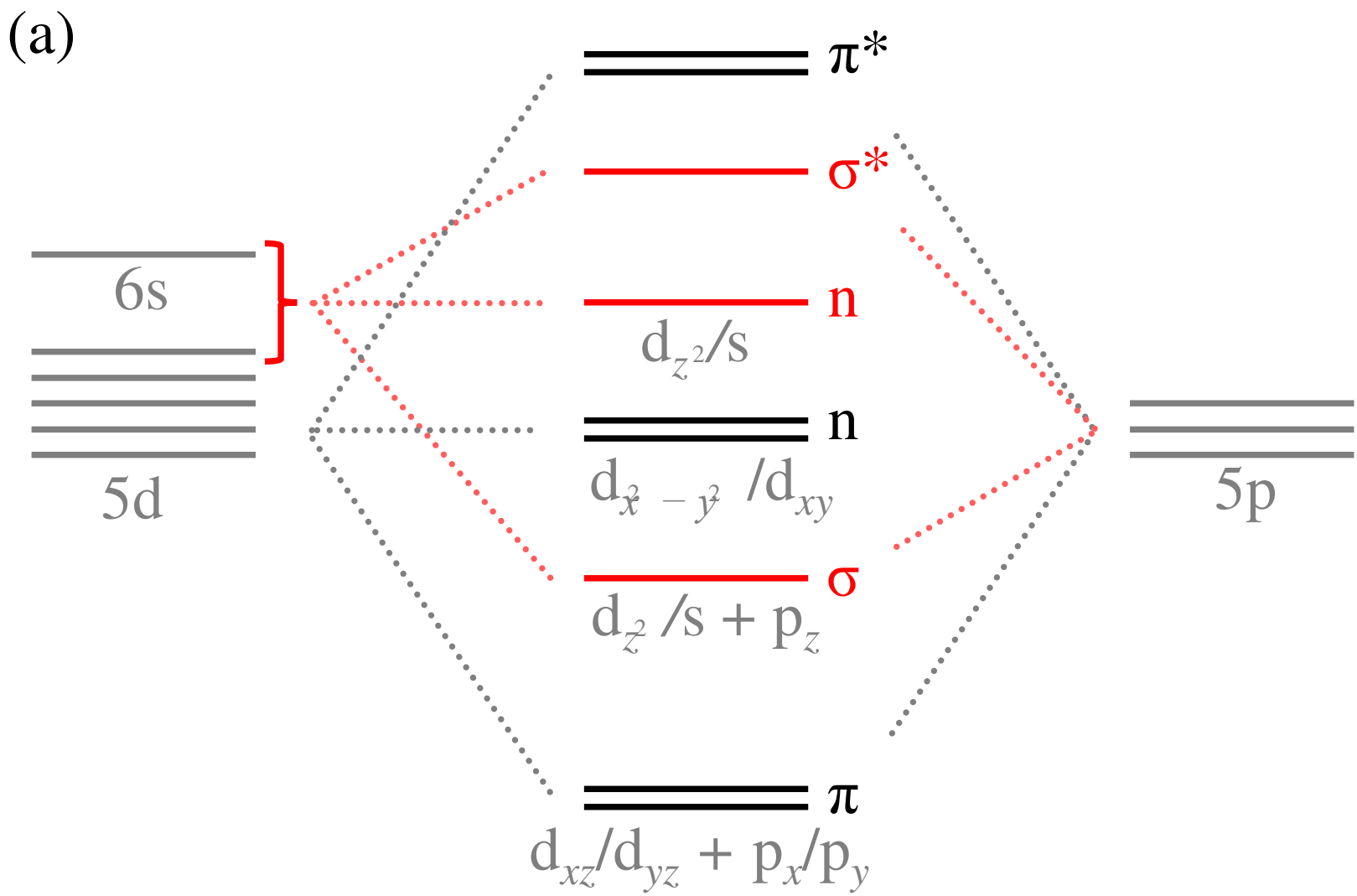
(a)
π*
σ*
6s
n
d_{z^2}/s
n
5d
$d_{x^2-y^2}$ /d_{xy}
5p
σ
d_{z^2} /s + p_z
π
d_{xz}/d_{yz} + p_x/p_y

(b)

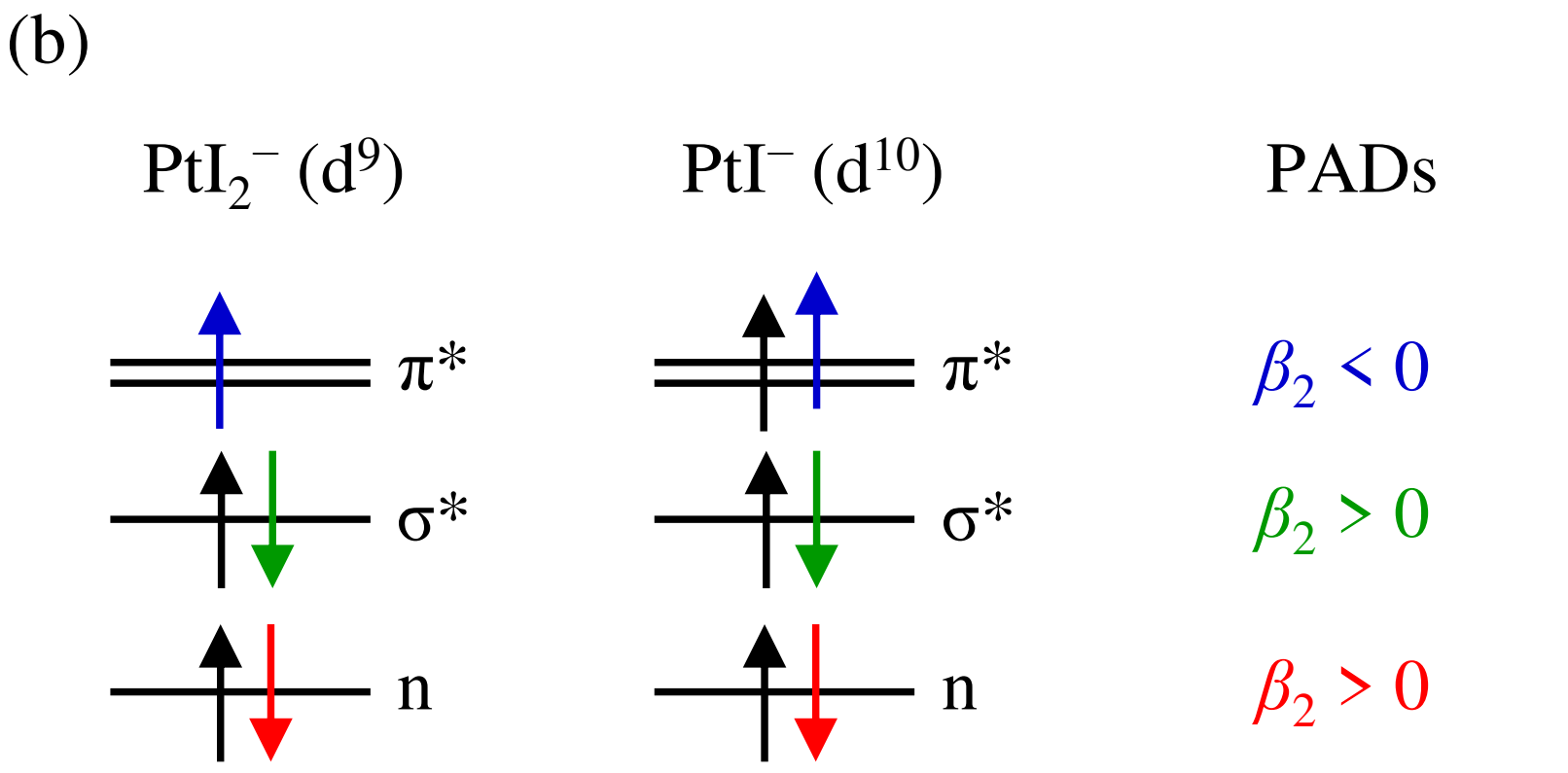
PtI_2^- (d^9)
PtI^- (d^{10})
PADs
π*
π*
$\beta_2 < 0$
σ*
σ*
$\beta_2 > 0$
n
n
$\beta_2 > 0$